Journal of Solid State Chemistry 184 (2011) 1749–1755

Contents lists available at ScienceDirect

Journal of Solid State Chemistry

journal homepage: www.elsevier.com/locate/jssc

Fabrication of carbon microcapsules containing silicon nanoparticles–carbon nanotubes nanocomposite by sol–gel method for anode in lithium ion battery

Joonwon Bae

Samsung Advanced Institute of Technology, Yong-In City 446-712, Gyeong-Gi Province, Republic of Korea

ARTICLE INFO

Article history:
Received 1 March 2011
Received in revised form
4 May 2011
Accepted 8 May 2011
Available online 19 May 2011

Keywords:
Carbon nanotube
Silicon nanoparticle
Microcapsule
Surfactant
Lithium battery anode

ABSTRACT

Carbon microcapsules containing silicon nanoparticles (Si NPs)–carbon nanotubes (CNTs) nanocomposite (Si-CNT@C) have been fabricated by a surfactant mediated sol–gel method followed by a carbonization process. Silicon nanoparticles–carbon nanotubes (Si-CNT) nanohybrids were produced by a wet-type beadsmill method. To obtain Si-CNT nanocomposites with spherical morphologies, a silica precursor (tetraethylorthosilicate, TEOS) and polymer (PMMA) mixture was employed as a structure-directing medium. Thus the Si-CNT/Silica-Polymer microspheres were prepared by an acid catalyzed sol–gel method. Then a carbon precursor such as polypyrrole (PPy) was incorporated onto the surfaces of pre-existing Si-CNT/silica-polymer to generate Si-CNT/Silica-Polymer@PPy microspheres. Subsequent thermal treatment of the precursor followed by wet etching of silica produced Si-CNT@C microcapsules. The intermediate silica/polymer must disappear during the carbonization and etching process resulting in the formation of an internal free space. The carbon precursor polymer should transform to carbon shell to encapsulate remaining Si-CNT nanocomposites. Therefore, hollow carbon microcapsules containing Si-CNT nanocomposites could be obtained (Si-CNT@C). The successful fabrication was confirmed by scanning electron microscopy (SEM) and X-ray diffraction (XRD). These final materials were employed for anode performance improvement in lithium ion battery. The cyclic performances of these Si-CNT@C microcapsules were measured with a lithium battery half cell tests.

1. Introduction

Recently, a large amount of interest has been attracted to the anode materials for lithium ion secondary batteries, which can replace conventional graphite anode to improve battery performance. Promising candidates for anode are Sn [1–7], Si [8–11], and LTO ($Li_4Ti_5O_{12}$) [12,13], and carbons with diverse structures [14–20]. Among those promising candidates, silicon has been investigated for use as a high-capacity anode material because its theoretical lithium capacity of approximately 4200 mAh/g ($Li_{4.4}Si$) is eleven times higher than the reversible capacity of graphite (372 mAh/g) [8], which is currently used as a most popular anode material. In spite of the high capacity, particle pulverization can be initiated by a large volume change ($>280\%$) during lithium charge (to Li_xSi) and discharge (to reform Si), which results in electrically disconnected smaller particles. This phenomenon causes a rapid decrease in cycling capability. Extensive researches have focused on reducing the volume change by making composites with a carbon material to prevent the aggregation of particle and to act as electrically connecting media between anode particles and the current collector when the particles are pulverized [21–30]. However, these methods lead to a decrease in the charge capacity to less than 1500 mAh/g after dozens of cycles. On the other hand, control of the volume change by tuning of the morphology of the Si has rarely been reported yet [31,32]. In addition, inherent low electrical conductivity of Si tends to degrade overall battery performance due to high impedance of electron flow during electrochemical process. Therefore, numerous ideas have been suggested to minimize the volume change and to increase the electrical conductivity [33–36]. Several remarkable approaches are the use of nanometer sized silicon [11,32,37] and preparation of composites with carbon materials such as amorphous carbon [28,29], aerogel [38], and carbon nanotubes [39–42].

Among carbon nanostructures, the application of CNTs in silicon-based anode materials has been attractive, owing to its advantageous effects such as excellent electrical conductivity and mechanical flexibility. However, Si-CNT nanocomposites have not yet been successfully developed due to several inherent difficulties. One critical problem is the high specific surface area of CNTs (100–1500 m^2/g depending on types), which would result in low

E-mail address: joonwonbae@gmail.com

0022-4596/$ - see front matter © 2011 Elsevier Inc. All rights reserved.
doi:10.1016/j.jssc.2011.05.012

initial coulombic efficiencies of less than 80% through the formation of a solid–electrolyte interface (SEI) on the surface of CNTs [43]. An initial efficiency higher than 85% in a half-cell is required as one of the most important criteria for the industrially acceptable full cell battery design. Another obstacle is the uniform dispersion of CNTs in composites. Most processes for composite preparations consist of the direct growth of CNTs or milling silicon with CNTs, but these methods have not yet been considered as reliable methodologies. In spite of these inherent obstacles, it is still lucrative to incorporate CNTs into silicon to prepare high capacity anode materials for lithium ion batteries.

In a previous article [44], it was reported that the Si-CNT nanocomposites produced by a cost-effective wet-type milling process followed by a thermal treatment exhibits a competitive electrochemical performance as an anode material in lithium ion battery. If we can confine Si-CNT nanocomposites into an external carbon shell to control the volume shrinkage/expansion of Si NPs, the cyclic performances and coulombic efficiencies of these Si-CNT nanocomposites are expected to improve dramatically. Therefore, in this study, carbon microcapsules containing Si-CNT nanocomposites (Si-CNT@C) have been fabricated by a surfactant mediated sol–gel process. The sol–gel process is of interest because of its mild processing conditions such as low temperature and pressure. Starting from metal alkoxides, the inorganic network is obtained via the hydrolysis and condensation reactions. The creation of strong covalent bonds between the organic and inorganic phases results in a reduced tendency of phase separation. Using these advantages, an intermediate polymer/silica layer, which is susceptible to a thermal treatment was incorporated on the surfaces of Si-CNT nanocomposites to generate Si-CNT/Silica-Polymer. Subsequently, carbon precursor polymer layer, which can be carbonized by a thermal treatment was incorporated onto the surfaces of preformed Si-CNT/Silica-Polymer to prepare Si-CNT/Silica-Polymer@Carbon Precursor microspheres. The intermediate silica/polymer readily disappears during carbonization and etching step resulting in the formation of an internal free space. The carbon precursor polymer should transform to carbon shell to encapsulate remaining Si-CNT nanocomposites. Therefore, hollow carbon microcapsules containing Si-CNT nanocomposites could be obtained (Si-CNT@C). This method is challenging and would pave a new way to improve the performances of a Si-CNT based anode electrode material in lithium ion battery.

2. Experimental

2.1. Materials

Silicon nanoparticles (Si NPs) with an average diameter of 100 nm was purchased from High Purity Chemical Co. (Japan) and used without further purifications. Multi-walled carbon nanotubes were purchased from Iljin Nanotech Inc. (Seoul, Korea) and used as received. Monomers, methyl methacrylate (MMA) and pyrrole (Py), surfactants such as sodium dodecyl sulfate (SDS), sorbitan monooleate (SPAN80), and initiator iron (III) chloride were purchased from Aldrich (Wisconsin, US) and used as received. Azobisbutylonitrile (AIBN) as an initiator was recrystallized from methanol. A silica precursor, tetraethylorthosilica (TEOS) and a catalyst, hydrochloric acid (HCl) were also received from Aldrich. All solvents such as octanol and ethanol were dried by a common method.

2.2. Fabrication of Si-CNT and Si-CNT@C

Si-CNT nanocomposites were prepared by a wet type beadsmill method. A mixture of Si nanopowder and CNT in a weight of 9:1 was crushed in octanol by beadsmill treatment (Ultra Apex Mill UAM-015, Kotobuki Ind. Co. Ltd., Japan). Fine slurry was obtained in the condition of 55 Hz for one or two hours using 0.1 mm sized zircornia beads. Then, Si-CNT nanocomposite was obtained by drying at 120 °C in air convection oven overnight.

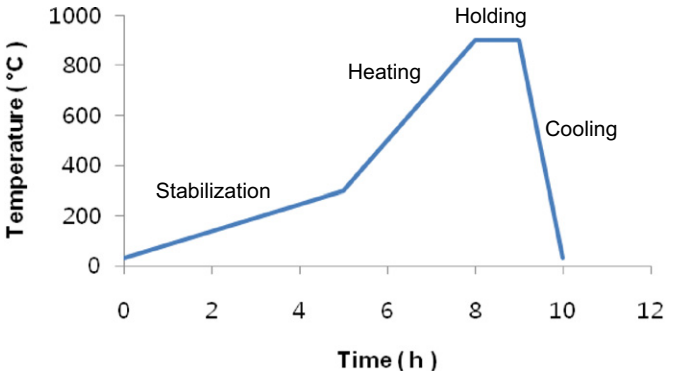

Fig. 1. Temperature profile for the carbonization of polymer microspheres. It is composed of stabilization (1 °C/min to 300 °C), heating (3 °C/min to 900 °C), holding, and natural cooling.

In a typical synthesis of Si-CNT@C microcapsules, Si-CNT (2.0 g) was mixed with octanol (0.5 g) and SPAN80 surfactant (0.25 g). This Si-CNT paste was dissolved in a SDS surfactant solution (0.5 g SDS in 50 mL distilled water) and stirred vigorously. Then an intermediate silica/polymer layer was formed by simultaneous reactions of polymerization of MMA monomer (2.0 g) with an initiator AIBN (0.01 g) and sol–gel reaction of TEOS (3.0 g) with 0.1 M HCl on the surfaces of Si-CNT at 75 °C for 3 h (Si-CNT/Silica-Polymer). Subsequently, a carbon precursor polymer layer, PPy was polymerized from Py monomer (0.5 g) with an initiator iron (III) chloride ($FeCl_3$, 1.0 g) at room temperature for 2 h (Si-CNT/Silica-Polymer@PPy). Carbonization of polymeric microcapsules containing Si-CNT at 900 °C under nitrogen atmosphere followed by silica etching with acid or base produced Si-CNT@C microcapsules. Fig. 1 shows the carbonization profiles employed in this study, which was composed of stabilization, heating, holding, and natural cooling. For the carbonization of polymer precursor, the stabilization step is critical.

2.3. Electrode preparation and half cell test

Carbon microcapsules containing Si-CNT (80 wt%) were mixed in a binder polyvinyldifluoride (PVDF, 20 wt%) and agitated. The solvent for PVDF was N-methylpyrrolidone (NMP). Then the paste was coated onto a 15 μm-thick copper foil and dried at 120 °C in a vacuum oven for 2 h. For half cell test, the electrode was pressed and punched in 12 mm diameter circle, then assembled in a coin-type cell (CR2016) with a lithium metal counter electrode, a polytetrafluoroethylene (PTFE) separator, and electrolyte (1.3 M $LiPF_6$ in EC/DEC 3:7 volume ratio, Cheil Industries Inc., Korea). Electrochemical measurements were performed at a constant current of 0.2 C rate in a voltage range of 0–1.5 V vs. Li/Li^+.

2.4. Characterizations

The morphology of microcapsules was observed using a Hitachi S4200 field emission scanning electron microscope (FE-SEM). High resolution transmission electron microscopy (TEM) was conducted using a 200 keV F20ST (FEI Company). X-ray diffraction patterns were recorded on a Rigaku RINT2200HF+ diffractometer with Cu $K\alpha$ radiation.

3. Results and discussion

Fig. 2 presents the SEM image of Si-CNT nanocomposite prepared by a beadsmill mixing. Silicon nanoparticles with an average diameter of 100 nm and knitted carbon nanotubes are homogeneously mixed as clearly seen in the image. After the beadsmilling of silicon particles with a micrometer scale, thin silicon platelets with an average thickness of tens of nanometer were obtained [44]. However, pulverization was not remarkable in this case.

The schematic synthetic procedure for fabrication of Si-CNT@C microcapsules is summarized in Fig. 3. First, Si-CNT nanocomposites prepared by a beadsmill method were mixed with octanol, which was selected as best solvent for a beadsmill treatment [44]. Then an amount of surfactant soluble in organic solvents, sorbitan monooleate (SPAN80) was added to stabilize the Si-CNT/SPAN80/octanol mixture in an aqueous SDS solution. It is generally known that the selection of counter surfactant is important and critical to produce very small droplets in an emulsion solution. It was revealed by our experiments that micelles from SPAN80 could retain their shapes in an aqueous SDS solution. The tests demonstrated that the spraying of a SPAN80 solution into a SDS solution generated spherical micelles.

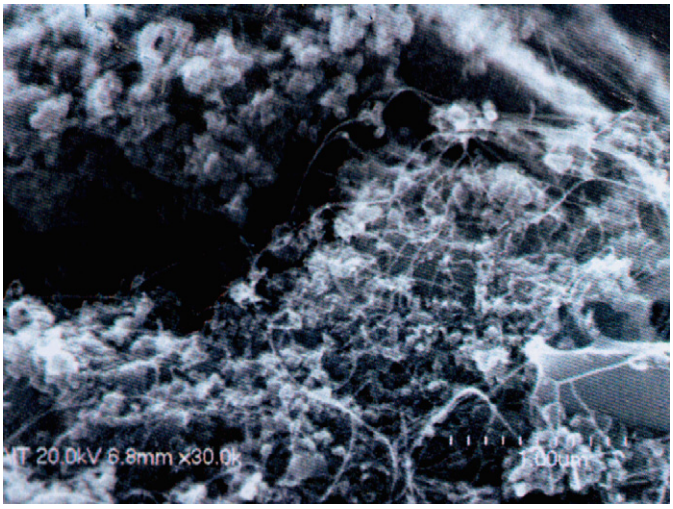

Fig. 2. Scanning electron microscopy image of Si-CNT composites prepared by a wet type beadsmill method.

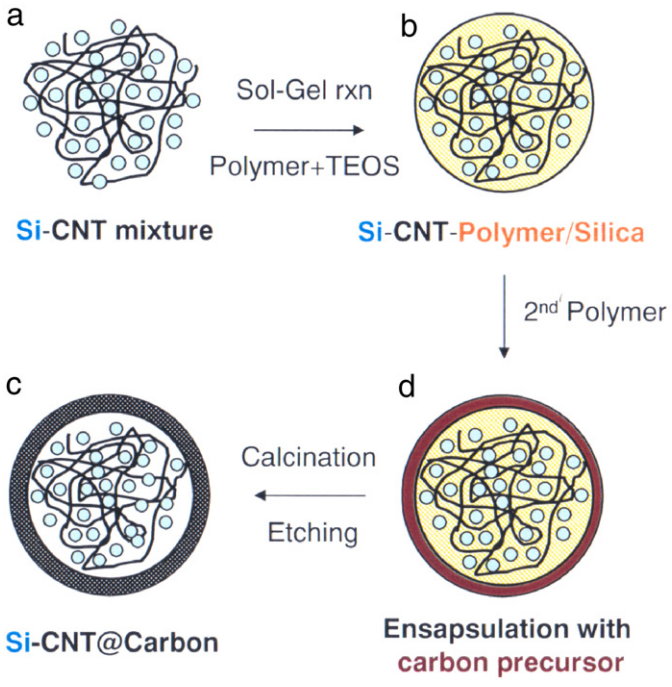

Fig. 3. Schematic procedure for the fabrication of polymer and carbon microcapsules containing Si-CNT nanocomposites.

Therefore, SPAN80 is a reasonable counter surfactant of SDS for the formation of microscale droplets in an emulsion system. In addition, it is important to apply a vigorous agitation to maintain the morphology of Si-CNT/SPAN80/octanol paste in a SDS solution. It was also confirmed that micelles from SPAN80 were stable under harsh electrospinning conditions [45]. On the other hand, the viscosities of SPAN80 and octanol can provide an adhesion promotion effect for CNT/SPAN80/octanol (Fig. 3a).

Then an intermediate silica-polymer medium, which decomposes easily during carbonization and acidic or basic etching step to generate internal space was introduced on the surfaces of Si-CNT nanocomposites. The monomer, methyl methacrylate shows affinities to surfactants SPAN80 and SDS. In addition, the surfaces of both Si NPs and CNTs are active sites for polymerization of methyl methacrylate. Therefore, polymerization must occur spontaneously with heating the mixture solution at a polymerization temperature. On the other hand, it is important to achieve weak acid catalyzed sol–gel reactions (hydrolysis and condensation) of silica precursor, TEOS to obtain a molecularly interconnected silica-polymer hybrid network. As the preparation of PMMA/silica sol–gel nanocomposite materials has been pursued extensively owing to their excellent optical properties and mechanical durability, it is well known that the two reactions, polymerization of MMA and sol–gel reaction of TEOS can happen simultaneously in surfactant solution containing Si-CNT, SPAN80 and SDS, and monomer MMA and TEOS [46,47]. One concern is that the shapes of resulting Si-CNT/Silica-Polymer microspheres might be ill-defined because the morphologies of Si-CNT nanocomposites are irregular. In addition, it is extremely difficult to prepare Si-CNT/Silica-Polymer microspheres with a narrow size distribution. However, the driving force for the formation of Si-CNT/Silica-Polymer microspheres is the balance in surface tension between two types of micelles derived from SPAN80 and SDS, respectively. These force balances at interfaces can promote the formation of roughly spherical microparticles (Fig. 3b).

Subsequently, a carbon precursor polymer layer such as PPy, which produced an external carbon shell encapsulating Si-CNT nanocomposite was polymerized onto the outer surfaces of pre-existing Si-CNT/Silica-Polymer microspheres to fabricate Si-CNT/Silica-Polymer@PPy. Previous experiments revealed that PMMA showed a favorable compatibility with PPy [48]. For PMMA-PPy, interfacial interaction and interdiffusion is known to be weak. This negligible interfacial diffusion is one of the most important prerequisites for the realization of hollow carbon microcapsules (Fig. 3c).

A subsequent thermal treatment under a controlled temperature profile produced Si-CNT@C microcapsules. The carbon spheres were obtained by a carbonization and a subsequent acidic or basic etching process. Because the precursors are polymeric, the stabilization step is very important. The molecular rearrangements of polymer chains and evaporation of low molecular weight components must happen in this slow elevation period (1 °C/min) leading to stable state for further heating. This process was carried out usually below 300 °C, which is a limitation for thermal resistances of most polymers. Carbon structures were produced during the heating process (3 °C/min) to target temperature, where the elimination of atoms (hydrogen, oxygen, and nitrogen) occurred simultaneously. Holding at target temperature a couple of hours

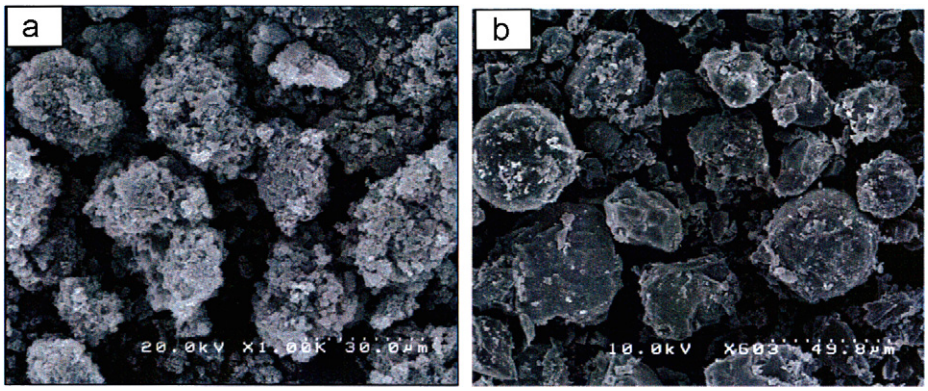

Fig. 4. (a) Scanning electron microscopy images of (a) Si-CNT/PMMA and (b) Si-CNT/Silica-Polymer microspheres.

followed by natural cooling provided spherical carbons. It would be clear that the breakage of polymer spheres during carbonization was insignificant. This finding supports the feasibility of our experimental procedure for carbon microsphere formation (Fig. 3d).

Fig. 4 displays the SEM images of Si-CNT/PMMA (a) and Si-CNT/Silica-Polymer (b) microspheres with tens of micrometer diameter. The overall morphologies of Si-CNT/PMMA and Si-CNT/Silica-Polymer are roughly spherical and there is a broad size distribution. The surfaces of microspheres are macroporous, which reflects the inherently irregular morphologies of Si-CNT nanocomposite. It has been almost impossible to encapsulate Si-CNT perfectly, but the incorporation of Si-CNT into confined state is meaningful for controlling volume expansion of Si NPs and providing electrical pathways between Si NPs. A closer look at the surface of microspheres reveals the presence of Si NPs, CNTs, and macropores, which are distributed homogeneously in each microsphere. These macropores can be filled with carbon precursor polymer like PPy leading to the generation of more symmetric spherical morphologies. Comparing the Si-CNT/Silica-Polymer with Si-CNT/PMMA, it is obvious that the exterior surfaces of Si-CNT/Silica-Polymer became clear and smooth. This fact indicates that the addition of silica network into Si-CNT/PMMA produced more rigid microparticles due to the condensation reaction of TEOS generating an interconnected structure.

The second polymerization of pyrrole with iron (III) chloride produced Si-CNT/Silica-Polymer@PPy microspheres shown in Fig. 5. It is conspicuous that the microspheres are composed of amorphous and spherical microparticles. If the surfaces of Si-CNT/Silica-Polymer microspheres were covered with a sufficiently thick layer of PPy, more spherical microparticles could be produced. On the contrary, nonuniform coating of PPy onto the surfaces of Si-CNT/Silica-Polymer microparticles generated microspheres with irregular shapes. Therefore, it is reasonable to conclude that Fig. 5 shows the typical image of Si-CNT/Silica-Polymer@PPy microspheres.

A thermal treatment of CNT/Silica-Polymer@PPy precursor with a controlled temperature profiles and a simple etching of silica with acid or base produced Si-CNT@C microcapsules presented in Fig. 6. It is difficult to recognize the remarkable structural changes during carbonization, because the overall texture in Fig. 5 is similar with that of Fig. 6. Moreover, the change in size before and after carbonization is not remarkable because the size of each Si-CNT@C microcapsule was determined by the core Si-CNT composite. Importantly, large scale aggregations of Si NPs or CNTs were not highly probable owing to the prevalent homogeneous distribution of silica network in Si-CNT, which means that the anode performances of Si-CNT@C are insignificantly affected by clusters of Si NPs or CNTs.

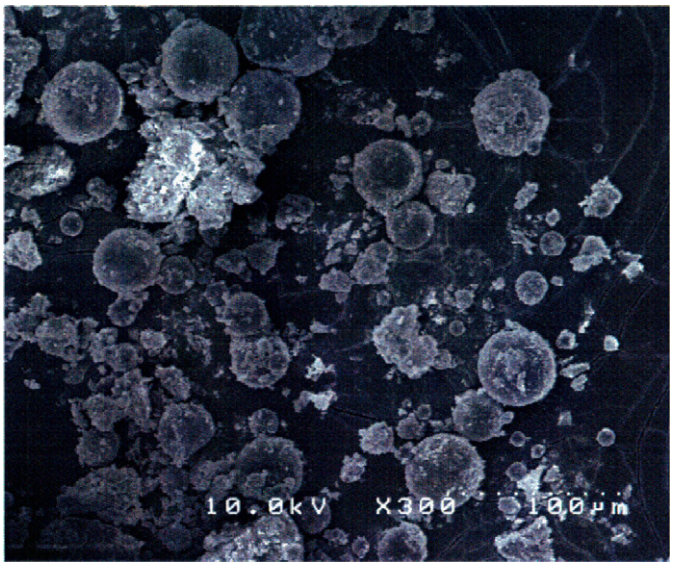

Fig. 5. Scanning electron microscopy image of Si-CNT/Silica-Polymer@PPy precursor.

Transmission electron microscopy (TEM) image (Fig. 6b) was taken to reveal the fine structure and atomic components inside microcapsules. Carbon shell and Si NPs are clearly observable from the TEM image. In addition, EDX analysis for internal components of carbon microcapsule indicated the presence of Si, O, C, and traces of S, Cl and Na (data not shown). This fact indicates that CNT, Si–C, and Si–O phases existed in the carbon microcapsules. The existence of Si–O phase can be understood by the presence of native oxide layer on Si surface. On the other hand, the formation of Si–C phase might be attributed to the carbonization of polymer precursor. In this image, the CNTs appeared as black points, which is undiscernable directly from cross-sectional TEM image.

The generation of internal spaces in Si-CNT@C microcapsules can be promoted by controlled carbonization of polymeric precursor. Jang and Oh [49] have revealed that the well-controlled carbonization of ultrasmall polypyrrole nanoparticles produced hollow fullerenes.When the polymeric precursors were heated slowly below 300 °C as shown in Fig. 1, the thickness of outer shell must decrease as carbonization proceeded due to volume shrinkage. At relatively slow heating speed below 300 °C, the formation of homogeneous outer carbon shell was energetically favorable because the induced stresses due to volume shrinkage were applied equally on the whole surface of microcapsule. But as the heating speed increased, more unstable structures might be produced. This is why stabilization step below 300 °C is very

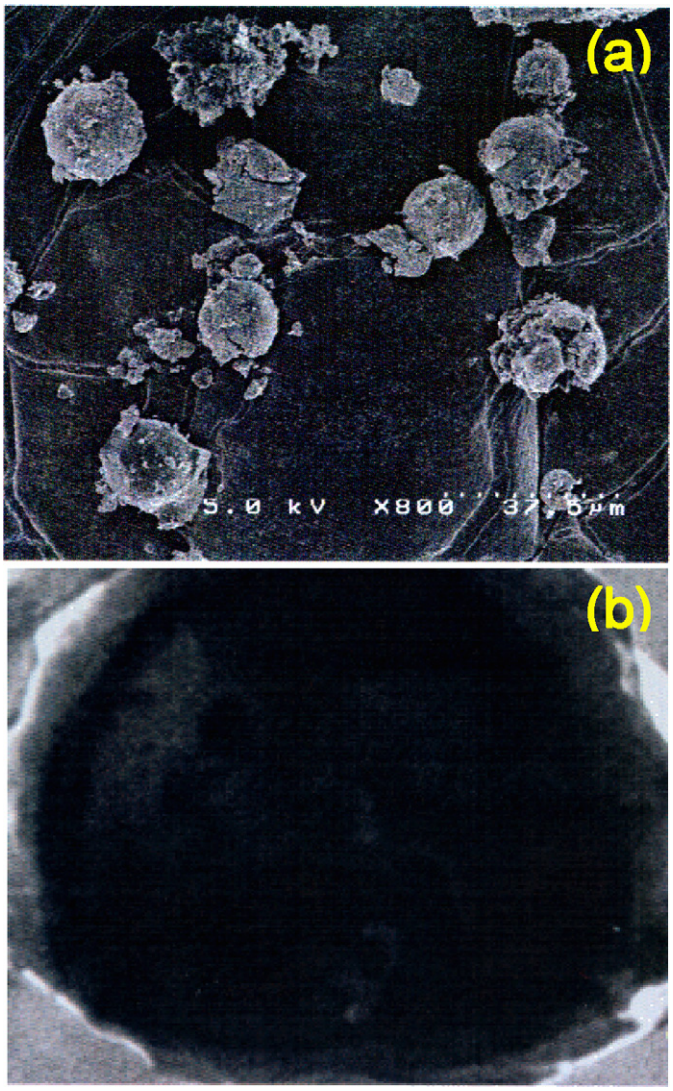

Fig. 6. Scanning electron microscopy (a) and cross-sectional transmission electron microscopy (b) images of Si-CNT@C microcapsules derived from Si-CNT/Silica-Polymer@PPy precursor.

important for the carbonization of polymeric precursor. For some microcapsules, the breakage of macropores might happen naturally. However, the fraction of disruption was found to be insignificant from the SEM and TEM images.

The successful formation of Si-CNT@C microcapsules was confirmed by X-ray diffraction spectrometer. Fig. 7 illustrates the typical XRD pattern of Si-CNT@C derived from Si-CNT/Silica-Polymer@PPy precursor. Characteristic peaks associated with Si, graphitic carbon from CNTs, and amorphous carbon from the carbon shell were clearly observed on the pattern in Fig. 7. It is noteworthy that the relative intensities of peaks for amorphous carbon are weak compared with those of graphite. This fact indicates that the average thickness of external carbon shell is low compared with the average diameter of Si-CNT@C microcapsules. This result is desirable for the performance improvement of Si-CNT@C as anode in lithium ion battery, because the flows of electrolytes or Li ions through the carbon shell layer can be promoted as the thickness decreases.

Fig. 8a exhibits the voltage profiles of the Si-CNT@C microcapsules (same as in Fig. 6) at 0.2 C rate between 1.5 and 0 V in coin-type half cells. At this rate, the first discharge and charge capacities were 1497 and 1195 mAh/g, respectively, which

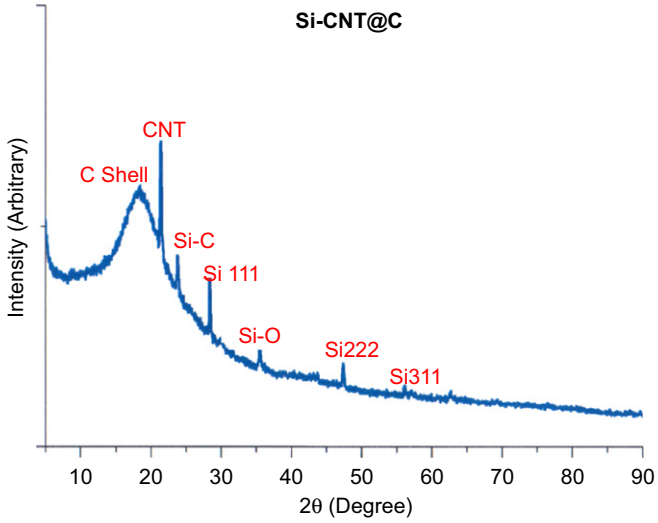

Fig. 7. XRD pattern of Si-CNT@C microcapsules.

indicates a coulombic efficiency of 80%. This is comparable with the Si nanowires (79% coulombic efficiency) [31]. This improved efficiency is associated with the presence of an external carbon shell, which may decrease the occurrence of side reactions with the electrolyte. On the other side, the first discharge and charge capacities were slightly lower than those of carbon microcapsules containing Si-CNT prepared without sol–gel precursor (1610 and 1314 mAh/g at 0.2 C). This is attributed to the presence of insulating silica as an intermediate state inside microcapsules, which provides reduced electrical connections for Si NPs. In addition, the coulombic efficiency of 80% is comparable with that of carbon microcapsules containing Si-CNT prepared without sol–gel precursor (78%). An irreversible capacity of 20% is due to the side reactions, where solvent and salt anions were reduced on the active site forming insoluble salts [50]. The other reason that contributes to the irreversible capacity is the presence of native oxides on the surfaces of Si NPs. The decomposition plateau of silicon oxides to Si and Li_2O must appear near 0.8 V [22]. Because the reversible capacity of the amorphous carbon is approximately 100 mAh/g [1], the capacity contribution from the carbon shell is negligible. The most important breakthrough of the use of silica is the improvement in capacity retention capability. For the carbon microcapsules containing Si-CNT prepared without sol–gel precursor, capacity retention at a rate of 0.2 C was as high as 50% after 25 cycles. However, for Si-CNT@C from Si-CNT/Silica-Polymer@PPy precursor, capacity retention at 0.2 C was higher than 75% and 65% after 25 and 30 cycles, respectively. This dramatic improvement is associated with the formation of more compact microspheres with the aid of condensation reaction of TEOS.

To substantiate the effect of silica, Si-CNT@C microcapsules were derived with addition of two times more amount of TEOS. The first discharge and charge capacities were 1410 and 1125 mAh/g, respectively, at a rate of 0.2 C, which indicates a coulombic efficiency of 79%. This value is significantly lower than those of sample in Fig. 8 (1497 and 1195 mAh/g). This fact indicates that the increase of TEOS addition deteriorates discharge and charge capacities. However, the capacity retention capability further improved by addition of TEOS. As clearly seen in Fig. 9, the capacity retention at a rate of 0.2 C was as high as 77% and 70% after 25 and 40 cycles, respectively, while a coulombic efficiency at 0.2 C was greater than 98% after 40 cycles. These facts systematically visualize the effect of silica on anode performance of Si-CNT@C derived from Si-CNT/Silica-Polymer@PPy precursor.

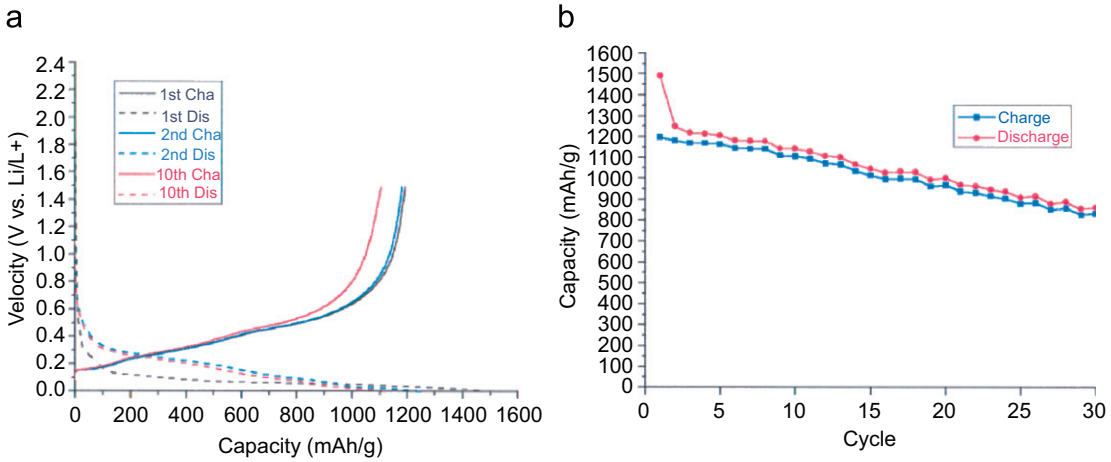

Fig. 8. (a) Voltage profiles and (b) plot of charge capacities versus cycle number of Si-CNT@C microcapsules from Si-CNT/Silica-Polymer@PPy precursor at 0.2 C rate between 0 and 1.5 V in coin-type half cells.

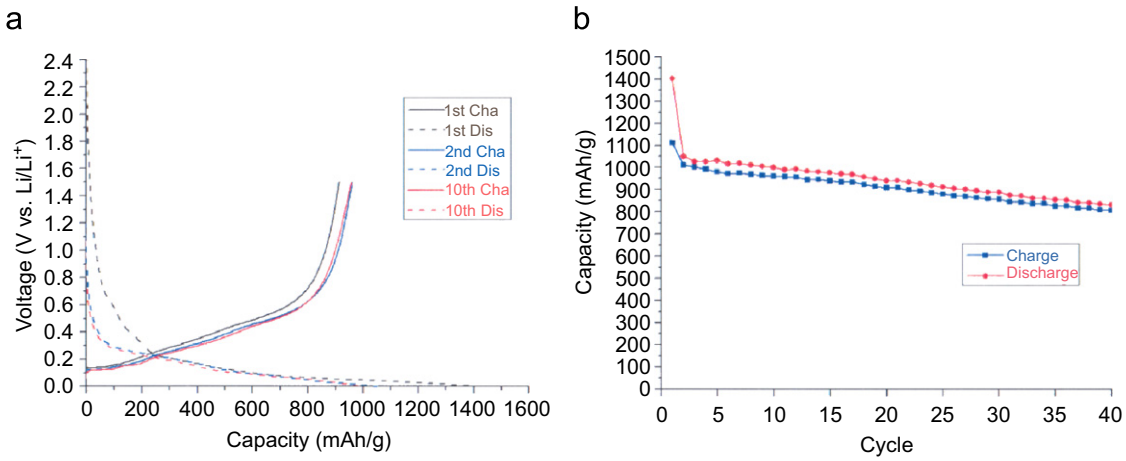

Fig. 9. (a) Voltage profiles and (b) plot of charge capacities versus cycle number of Si-CNT@C microcapsules from Si-CNT/Silica-Polymer@PPy precursor prepared with two times more amount of TEOS at 0.2 C rate between 0 and 1.5 V in coin-type half cells.

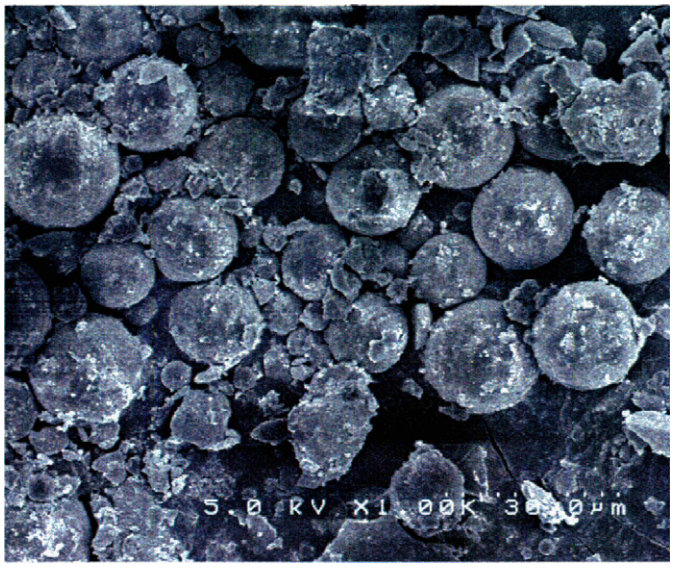

Fig. 10. Scanning electron microscopy image of Si-CNT@C microcapsules shown in Fig. 8 after 50 Li ion charge/discharge processes.

It is meaningful to observe the morphology of Si-CNT@C microcapsules after lithium battery half cell test. Fig. 10 shows the SEM image of Si-CNT@C microcapsules after 50 charge/discharge cycles (same sample as in Fig. 8). The most remarkable difference between before and after battery cycles was the presence of salt or other components outside microcapsules. This is due to the side reaction with electrolyte or salt formation. However, the overall morphology did not change considerably by Li charge/discharge process.

4. Conclusion

Polymer and carbon microcapsules containing silicon nanoparticle-carbon nanotube composite (Si-CNT@C) were successfully fabricated by a surfactant mediated sol–gel method by a carbonization process. More rigid and spherical polymeric microspheres could be prepared with the aid of sol–gel reaction leading to molecularly interconnected networks. The resulting Si-CNT@C microcapsules had internal free space generated from sol–gel silica-polymer network for accommodating volume expansion/shrinkage of silicon nanoparticles during lithium ion charge/discharge process. These Si-CNT@C microcapsules were successfully incorporated as anode in lithium ion batteries. They showed a comparably high reversible capacity and a coulombic efficiency (~80%). The use of silica as an intermediate layer could improve the capacity retention capability of Si-CNT@C microcapsules significantly. The morphology of Si-CNT@C microcapsules were retained after 50 cycles. This work

can promote subsequent research on Si-CNT hybrid materials for practical commercialization.

References

[1] M. Noh, Y. Kwon, H. Lee, J. Cho, Y. Kim, M.G. Kim, Chem. Mater. 17 (2005) 1926.
[2] K.T. Lee, Y.S. Jung, S.M. Oh, J. Am. Chem. Soc. 125 (2003) 5652.
[3] W.-M. Zhang, J.-S. Hu, Y.-G. Guo, S.-F. Zheng, L.-S. Zhong, W.-G. Song, L.-J. Wan, Adv. Mater. 20 (2008) 1160.
[4] X.W. Lou, C.M. Li, L.A. Archer, Adv. Mater. 21 (2009) 1.
[5] D. Deng, J.Y. Lee, Angew. Chem. Int. Ed. 48 (2009) 1660.
[6] G. Chen, Z. Wang, D. Xia, Chem. Mater. 20 (2008) 6951.
[7] I. Grigoriants, L. Sominski, H. Li, I. Ifargan, D. Aurbach, A. Gedanken, Chem. Commun. (2005) 921.
[8] U. Kasavajjula, C. Wang, A.J. Appleby, J. Power Sources 163 (2007) 1003 163.
[9] H. Kim, J. Cho, Nano Lett. 8 (2008) 3688.
[10] J.-H. Kima, H.-J. Sohn, H. Kim, G. Jeong, W. Choi, J. Power Sources 170 (2007) 456.
[11] D.-K. Kang, J.A. Corno, J.L. Gole, H.–C. Shin, J. Electrochem. Soc. 155 (2008) A276.
[12] Y.-G. Guo, Y.-S. Hu, W. Sigle, J. Maier, Adv. Mater. 19 (2007) 2087.
[13] D.-W. Wang, H.-T. Fang, F. Li, Z.-G. Chen, Q.-S. Zhong, G.Q. Lu, H.-M. Cheng, Adv. Funct. Mater. 18 (2008) 3787.
[14] Y. Huang, H. Cai, D. Feng, D. Gu, Y. Deng, B. Tu, H. Wang, P.A. Webleyb, D. Zhao, Chem. Commun. (2008) 2641.
[15] I. Mochida, C.-H. Ku, S.-H. Yoon, Y. Korai, J. Power Sources 75 (1998) 214.
[16] G.T. Teixidor, R.B. Zaouk, B.Y. Park, M.J. Madou, J. Power Sources 183 (2008) 730.
[17] J.R. Dahn, T. Zheng, Y. Liu, J.S. Xue, Science 270 (1995) 590.
[18] K. Sato, M. Noguchi, A. Demachi, N. Oki, M. Endo, Science 264 (1994) 556.
[19] F. Bonino, S. Brutti, P. Reale, B. Scrosati, L. Gherghel, J. Wu, K. Muellen, Adv. Mater. 17 (2005) 743.
[20] L. Kavan, Chem. Rev. 97 (1997) 3061.
[21] C.S. Wang, G.T. Wu, X.B. Zhang, Z.F. Qi, W.Z. Li, J. Electrochem. Soc. 145 (1998) 2751.
[22] H.Y. Lee, S.M. Lee, Electrochem. Commun. 6 (2004) 465.
[23] G.X. Wang, J. Yao, H.K. Liu, Electrochem. Solid-State Lett. 7 (2004) A250.
[24] H. Li, X. Huang, L. Chen, Z. Wu, Y. Liang, Electrochem. Solid-State Lett. 2 (1999) 547.
[25] I.S. Kim, P.N. Kumta, J. Power Sources 136 (2004) 145.
[26] G.X. Wang, J.H. Ahn, J. Yao, S. Bewlay, H.K. Liu, Electrochem. Commun. 6 (2004) 689.
[27] N. Dimov, S. Kugino, M. Yoshio, J. Power Sources 136 (2004) 108.
[28] Y.S. Hu, R. Demir-Cakan, M.M. Titirici, J.O. Mueller, R. Schloegl, M. Antonietti, J. Maier, Angew. Chem. Int. Ed. 47 (2008) 1645.
[29] S.H. Ng, J. Wang, D. Wexler, K. Konstantinov, Z.-P. Guo, H.K. Liu, Angew. Chem. Int. Ed. 45 (2006) 6896.
[30] M. Holzapfel, H. Buqa, W. Scheifele, P. Nov_k, F.-M. Petrat, Chem. Commun. (2005) 1566.
[31] C.K. Chan, H. Peng, G. Liu, K. Mcilwrath, X.F. Zhang, R.A. Huggins, Y. Cui, Nat. Nanotechnol. 3 (2008) 31.
[32] H. Ma, F. Cheng, J. Chen, J. Zhao, C. Li, Z. Tao, J. Liang, Adv. Mater. 19 (2007) 4067.
[33] F. Su, X.S. Zhao, Y. Wang, J. Zeng, Z. Zhou, J.Y. Lee, J. Phys. Chem. B 109 (2005) 20200.
[34] T. Kim, Y.H. Mo, K.S. Nahm, S.M. Oh, J. Power Sources 162 (2006) 1275.
[35] J.-H. Lee, W.-J. Kim, J.-Y. Kim, S.-H. Lim, S.-M. Lee, J. Power Sources 176 (2008) 353.
[36] S.H. Ng, J. Wang, D. Wexler, S.Y. Chew, H.K. Liu, J. Phys. Chem. C 111 (2007) 11131.
[37] K. Peng, J. Jie, W. Zhang, S.–T. Lee, Appl. Phys. Lett. 93 (2008) 033105.
[38] T. Hasegawa, S.R. Mukai, Y. Shirota, H. Tamon, Carbon 42 (2004) 2573.
[39] J.Y. Eom, J.W. Park, H.S. Kwon, S. Rajendran, J. Electrochem. Soc. 153 (2006) A1678.
[40] Z.S. Wen, J. Yang, B.F. Wang, K. Wang, Y. Lui, Electrochem. Commun. 8 (2006) 51.
[41] Y. Zhang, X.G. Zhange, H.L. Zhang, Z.G. Zhao, F. Li, C. Liu, H.M. Cheng, Electrochim. Acta 51 (2006) 4994.
[42] W. Wang, P.N. Kumta, J. Power Sources 172 (2007) 650.
[43] L.F. Nazar, O. Crosnier, in: G.-A. Nazri, G. Pistoria (Eds.), Lithium Batteries Sciences and Technology, Kluwer Academic/Plenum, Boston, 2004, p. 112.
[44] J. Lee, J. Bae, J. Heo, I.T. Han, S.N. Cha, D.K. Kim, M. Yang, H.S. Han, W.S. Jeon, J. Chung, J. Electrochem. Soc. 156 (2009) A905.
[45] N. Tonanon, W. Intarapanya, W. Tanthapanichakoon, H. Nishihara, S.R. Mukai, H. Tamon, J. Porous Mater 15 (2008) 265.
[46] H.-C. Kuan, S.-L. Chiu, C.-H. Chen, C.-F. Kuan, C.-L. Chiang, J. Appl. Polym. Sci. 113 (2009) 1959.
[47] N. Tonanon, W. Intarapanya, W. Tanthapanichakoon, H. Nishihara, S.R. Mukai, H. Tamon, Carbon 41 (2003) 2981.
[48] J. Jang, J. Oh, Adv. Funct. Mater. 15 (2005) 494.
[49] J. Jang, J. Oh, Adv. Mater. 16 (2004) 1650.
[50] D. Aurbach, A. Nimberger, B. Markovsky, E. Levi, E. Sominski, A. Gedanken, Chem. Mater. 14 (2002) 4155.